1–18, 2023

Evaluating Adversarial Robustness of Low dose CT Recovery

Kanchana Vaishnavi Gandikota KANCHANA.GANDIKOTA@UNI-SIEGEN.DE
Paramanand Chandramouli PARAMANAND.CHANDRAMOULI@UNI-SIEGEN.DE
Hannah Droege HANNAH.DROEGE@UNI-SIEGEN.DE
Michael Moeller MICHAEL.MOELLER@UNI-SIEGEN.DE
Department of Computer Science
University of Siegen

Abstract

Low dose computer tomography (CT) acquisition using reduced radiation or sparse angle measurements is recommended to decrease the harmful effects of X-ray radiation. Recent works apply deep networks to the problem of low dose, sparse view CT recovery. These methods have demonstrated high quality reconstructions, surpassing classical approaches on benchmark CT recovery datasets. However, their robustness needs be carefully evaluated before use in clinical applications. In this paper, we evaluate the robustness of different deep learning approaches as well as classical methods for CT reconstruction to untargeted and localized adversarial attacks. Our results demonstrate that deep networks, including model based networks encouraging data consistency are more susceptible to untargeted attacks than classical approaches. On the other hand, both classical approaches and deep networks can get affected by perturbations aiming to change a small localized region in the reconstructed CT image. Interestingly, we observe that data consistency is hardly affected in these local attacks. Our results motivate the need for better regularization in CT recovery networks to improve robustness.

Keywords: Computer tomography, robustness, adversarial attacks, image reconstruction.

1. Introduction

Computer tomography (CT), is a non-invasive imaging technique used to diagnose a wide range of medical conditions. The procedure involves recording attenuated X-ray radiation projected at different angles by a scanner rotating around a target. The recorded measurements are arranged into a sinogram, from which a CT image is reconstructed. While the accuracy and resolution of CT images improves with number of X-ray beams used, exposure of patients to X-rays poses serious health risks. To reduce the effect of ionizing X-ray radiation, different solutions to low-dose CT acquisition have been proposed under the ALARA (as low as reasonably achievable) principle (Slovis, 2002; Newman and Callahan, 2011). These protocols can be broadly classified into two categories- i) adjusting the settings on the CT scanner tube to reduce total number of X-ray photons ii) recording measurements from fewer projection angles. However, there exists a trade-off between dose reduction during CT acquisition and diagnostic quality. Lower number of X-ray photons degrades reconstruction quality due to increased image noise level. On the other hand, CT recovery from fewer projection angles can suffer from severe artefacts. Further, sparse-view CT is an ill-posed problem, and there can be many valid solutions for the same measurement.

Traditional approaches to ill-posed CT recovery impose suitable priors such as total variation (Sidky et al., 2006; Chen et al., 2013) in a variational reconstruction algorithm.

Recent works (Chen et al., 2017; He et al., 2020) train deep networks for sparse view CT recovery. While deep networks achieve impressive performance, they lack convergence guarantees provided by classical approaches. Further, sensitivity of deep neural networks to adversarial examples (Szegedy et al., 2014; Goodfellow et al., 2015) is a serious concern when using such deep networks for clinical applications. In this paper, we investigate the robustness of classical methods, fully learned, and model inspired deep networks to norm bounded additive adversarial perturbations. Our experiments show that deep networks, including the model inspired ones are significantly more susceptible to untargeted adversarial examples than classical methods. Yet, both classical approaches and deep learning methods are sensitive to localized adversarial attacks aiming to alter the visual appearance of a small diagnostically relevant regions. Such local attacks are possible with very low amounts of adversarial noise and high data consistency with original measurement, indicating that multiple diagnostically different solutions can be obtained with high data consistency. We also observe that even poor reconstructions due to untargeted attacks display a reasonable data consistency with their input, typical of unregularized solutions. These observations motivate the need for better regularization for image recovery networks.

2. Background and Related Work

2.1. CT Acquisition and Reconstruction

CT acquisition involves projecting X-ray beams from different angles and recording the attenuation of X-ray as a a sinogram. The forward operator is given by the 2D Radon transform (Radon, 1986) which models the attenuation of the radiation passing through the target by calculating line integral along the path of X-ray beam. The measurement, which is a sinogram consists of the recorded integrals for different distances and measurement angles. Since the Radon transform is linear, the measurement process can be written as:

$$f = Au + n \tag{1}$$

where f, A, u, n represent the sinogram, forward Radon transform, the ground truth image and measurement noise respectively. The aim of CT reconstruction is to recover a CT image $\hat{u}$ from the sinogram f. Linearly filtering in Fourier space, commonly referred to as filtered back projection (FBP) (Feldkamp et al., 1984), is one standard classical approach to CT recovery. Variational approaches (Sidky et al., 2006; Chen et al., 2013) find a minimizer of the energy function

$$\hat{u} = \arg\min_u \frac{1}{2}\|Au - f\|^2 + R(u) \tag{2}$$

for a suitable regularizer $R(u)$ such as the total variation $\|\nabla u\|_{2,1}$. Recent approaches successfully employ deep learning for the ill-posed image reconstruction problems. In the following, we review existing deep learning based solutions to CT reconstruction.

2.2. Deep learning for Image and CT Reconstruction

Deep learning approaches to image reconstruction tasks encompass a wide array of methods: *i) fully learned methods* directly invert the forward imaging model (Zhu et al., 2018; Kupyn

et al., 2018). Examples for CT recovery include iRadonmap (He et al., 2020) and ADAPTIVE-Net (Ge et al., 2020), which also learn the filtered back projection operation

$$\hat{u} = \mathcal{N}(f) \tag{3}$$

ii) learning deep neural network post-processors denoise an initial reconstruction such as output from the filtered-back-projection operator $B^\dagger(\cdot)$ (Chen et al., 2017; Jin et al., 2017; Yang et al., 2018; Zhang et al., 2018; Pelt et al., 2018; Kuanar et al., 2019)

$$\hat{u} = \mathcal{N}(B^\dagger(f)) \tag{4}$$

iii) unrolled optimization networks are end-to-end trained model inspired neural networks which unroll fixed iterations of algorithms such as gradient descent, primal-dual hybrid gradient, projected gradient descent with learned parameters (Adler and Öktem, 2017; Aggarwal et al., 2018; Adler and Öktem, 2018). Closely related is the method of using trained networks for projection or proximal step (He et al., 2018; Gupta et al., 2018).
iv) use of trained/untrained neural network priors in a variational inference (Bora et al., 2017; Rick Chang et al., 2017; Meinhardt et al., 2017; Ulyanov et al., 2018; Heckel et al., 2019). For CT recovery, (Baguer et al., 2020) use untrained neural network prior (Ulyanov et al., 2018), and (Song et al., 2022) use generative models trained on CT images.

In this work, we analyze the adversarial robustness of the deep learning paradigms $i) - iii)$, which can recover CT images in a single forward pass. In addition, we consider the classical approaches of filtered back projection and energy minimization with TV prior. We exclude $iv)$ in our experiments due to high computational complexity.

2.3. Adversarial Attacks on Image Reconstruction

Adversarial attacks refer to a phenomenon where a carefully crafted imperceptible change in the input causes a catastrophic failure of neural networks. Starting from (Szegedy et al., 2014; Goodfellow et al., 2015) a lot of research was done on creating strong adversarial examples and defense mechanisms to improve adversarial robustness of networks, mainly in the context of classification networks. Recent works (Antun et al., 2020; Raj et al., 2020) have demonstrated the susceptibility of image reconstruction networks to adversarial attacks. While (Antun et al., 2020) investigate instabilities to perturbations in the image domain, (Raj et al., 2020) consider adversarial examples in measurement domain and propose adversarial training to improve robustness. However, these works consider mainly non-targeted attacks for networks doing direct inversion or post-processing. A few recent works (Choi et al., 2019; Gandikota et al., 2022) also investigated the adversarial robustness of image restoration methods. In the context of MRI recovery, (Cheng et al., 2020) show that networks can fail to recover tiny features under adversarial attacks and perform robust training to increase the network's sensitivity to these small features. (Darestani et al., 2021; Morshuis et al., 2022) show that adversarial perturbations can alter diagnostically relevant regions in recovered MRI images. In the context of CT recovery, (Huang et al., 2018) perform preliminary investigations whether additive adversarial perturbations can lead to incorrect reconstruction of an existing lesion. Closely related to our work, (Genzel et al., 2022) investigate the adversarial robustness of different approaches for CT recovery. They, however, do not evaluate on medical CT data, and mainly considered untargeted attacks,

with some preliminary experiments on targeted changes indicating that reconstruction networks are largely robust to targeted changes. In contrast, we investigate susceptibility of CT recovery methods to both untargeted attacks and localized targeted adversarial attacks in diagnostically relevant regions in thoracic CT scans from (Armato III et al., 2011).

3. Analyzing Stability of (CT) Image Recovery

Ideally, the recovery algorithm or network $\mathcal{N}$ should have a small Lipschitz constant L so that small changes in the input produce only small bounded changes in the reconstruction,

$$\|\mathcal{N}(f_1) - \mathcal{N}(f_2)\| \leq L\|f_1 - f_2\|. \tag{5}$$

However, exactly computing Lipschitz constant for neural networks has extremely high computational complexity (Jordan and Dimakis, 2020) even for moderately sized neural networks, and recent works (Combettes and Pesquet, 2020; Jordan and Dimakis, 2020; Huang et al., 2021) instead estimate an upper bound on Lipschitz constant. On the other hand, it is easier to analyze the stability of classical approaches. The stability of the standard linear techniques can be analyzed via the singular values of the reconstruction operator, see, e.g. (Bauermeister et al., 2020) for learning linear reconstructions in such a context. For nonlinear variational energy minimization approaches, a stability estimate shown in (Burger et al., 2007) is

$$\|f_1 - f_2\|^2 \geq \|Au_1 - Au_2\|^2 + 2\langle p_1 - p_2, u_1 - u_2\rangle, \quad p_1 \in \partial R(u_1),\ p_2 \in \partial R(u_2), \tag{6}$$

where the term $\langle p_1 - p_2, u_1 - u_2\rangle$ is called the 'symmetric Bregman distance' with respect to the convex regularizer R.

3.1. Adversarial Attacks on CT recovery

Adversarial attacks on image reconstruction methods make small changes to the inputs causing unpredictable large changes in the output. In this work, we consider robustness to tiny norm bounded additive perturbations in the measurement domain. We assume that the parameters of the neural network $\mathcal{N}$ or the recovery algorithm is fully known to the attacker.
Untargeted Attacks: Here the aim is to find an additive perturbation in the measurement domain that maximizes the reconstruction error subject to L_p constraints on the perturbation,

$$\delta_{adv} = \underset{\delta \in \mathrm{R}^m}{\operatorname{argmax}} \|\mathcal{N}(f+\delta) - \mathcal{N}(f)\|_2 \text{ s.t. } \|\delta\|_p \leq \epsilon. \tag{7}$$

Localized Attacks: Here the goal is to find an additive L_p norm constrained perturbation that produces a localized change in the reconstruction. Specifically, we investigate whether a tiny perturbation changes the visual appearance in the localized region to cause a classifier to change the predicted malignancy of a nodule. As this classification is also susceptible to adversarial attacks without actual change in the malignancy level in the region of interest, we utilize an adversarially trained classification network $\mathcal{N}_\theta$ pre-trained for classifying nodules in chest CT. Our localized attack can be formulated as:

$$\delta_{adv} = \underset{\delta \in \mathrm{R}^m}{\operatorname{argmax}} E(\mathcal{N}_\theta\left(g_c\left(\mathcal{N}(f+\delta)\right)\right), y) \text{ s.t. } \|\delta\|_p \leq \epsilon. \tag{8}$$

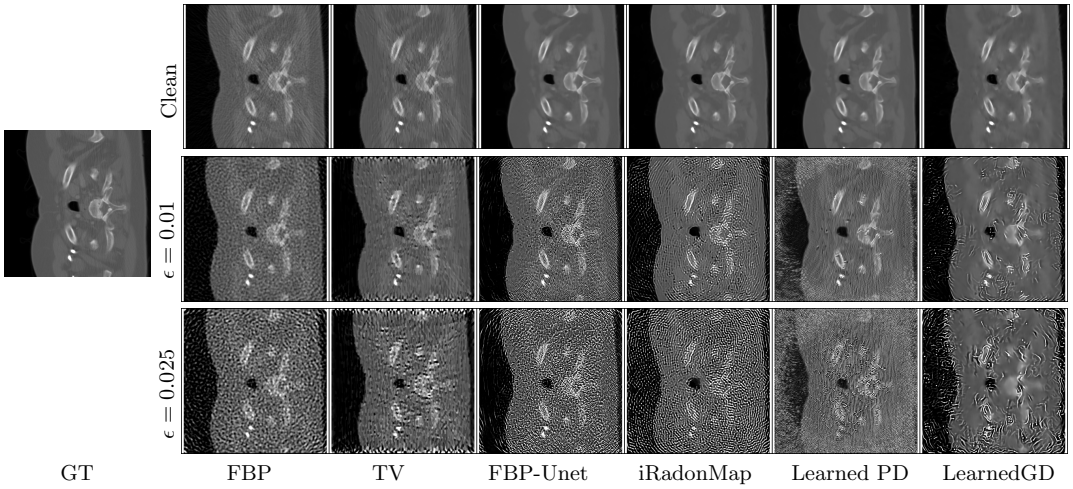

Figure 1: Untargeted attack on CT reconstruction methods for ϵ values 0.01 and 0.025.

Method	$\hat{u}$ PSNR/SSIM/d_{Breg}	$(A\hat{u}, f)$ PSNR	ϵ	$\hat{u}_\delta$ PSNR/SSIM/d_{Breg}	$(A\hat{u}_\delta, f)$ PSNR	$(A\hat{u}_\delta, f_\delta)$ PSNR	(f, f_δ) PSNR	L_b Empir
FBP	30.37/0.738/0.018	33.82	0.01	25.18/0.448/0.029	33.36	33.37	40.20	15.03
			0.025	18.68/0.194/0.049	31.47	31.43	32.51	
			0.05	13.02/0.074/0.081	28.46	28.34	26.91	
TV	31.62/0.763/0.018	36.52	0.01	25.20/0.615/0.026	35.62	35.72	40.36	16.52
			0.025	18.32/0.365/0.044	32.51	33.24	32.71	
			0.05	12.99/0.150/0.077	28.66	30.01	27.22	
FBP-Unet	35.47/0.837/0.013	36.47	0.01	18.39/0.287/0.081	35.06	35.71	40.28	46.71
			0.025	12.18/0.095/0.152	29.82	30.95	32.77	
			0.05	7.38/0.034/0.227	24.86	25.93	27.39	
iRadonMap	33.94/0.810/0.014	36.03	0.01	17.98/0.326/0.062	29.62	29.90	40.22	43.80
			0.025	10.85/0.084/0.140	24.07	24.51	32.60	
			0.05	6.24/0.026/0.215	21.50	21.98	27.16	
LearnedPD	35.73/0.842/0.012	36.46	0.01	9.47/0.164/0.230	25.27	25.50	40.48	143.39
			0.025	3.38/0.030/0.467	23.05	23.38	32.95	
			0.05	0.36/ 0.008/0.623	28.28	28.72	27.17	
LearnedGD	34.55/0.815/0.014	36.43	0.01	21.14/0.504/0.036	35.18	35.62	40.39	30.48
			0.025	13.90/0.291/0.069	31.62	32.82	32.80	
			0.05	8.64/0.180/0.099	28.11	29.64	27.50	

Table 1: Comparison of robustness to untargeted attacks on different CT reconstruction methods using 20 attack iterations on first 100 samples LoDoPAB testset.

where $g_c(\cdot)$ crops the region of interest, and $y = \mathcal{N}_\theta\left(g_c\left(\mathcal{N}(f)\right)\right)$ is the predicted label for the region of interest in the clean reconstruction. $E(\cdot)$ refers to the energy function (loss) to be maximized for binary classification of nodules, which is the binary cross entropy loss. In this work we consider L_∞ norm bounded perturbations. Similar attacks can also be defined for other L_p norm bounded perturbations. We solve the constrained optimization problems (7), (8) using the projected gradient descent (PGD) algorithm (Madry et al., 2018), with gradient updates using the Adam optimizer (Kingma and Ba, 2015).

4. Experiments and Results

We conduct experiments with low-dose parallel beam (LoDoPaB) CT dataset (Leuschner et al., 2021), consisting of data pairs of simulated low-intensity measurements for sampling 513 out of 1000 parallel beams and corresponding ground truth human chest CT images from the LIDC/IDRI dataset(Armato III et al., 2011). We evaluate the robustness of the following approaches: i) Filtered back projection(FBP) ii) FBP-Unet (Chen et al., 2017) post-processing FBP outputs, iii) iRadonmap(He et al., 2020), which also learns back projection in addition to pre-processing, iv) LearnedGD, learned gradient descent v) Learned Primal Dual(Adler and Öktem, 2018) vi) Total Variation regularization. For the learned methods ii)-v), we use the pretrained models[1] from (Baguer et al., 2020) trained on the full training set excluding iRadonmap (which we trained ourselves to full convergence). For FBP, we employ the Hann filter with low-pass cut-off of 0.6410, the best setting for this dataset in (Baguer et al., 2020). When attacking FBP-Unet Equation (4), we also backpropagate through $B^{\dagger}(\cdot)$. For TV minimization, we used 500 gradient descent steps, with a TV weight of 1e-3, and the attack backpropagates through all the gradient descent steps. For the localized attacks, we obtain the locations of regions of interest corresponding to ground truth from the LIDC-IDRI dataset (Armato III et al., 2011). We exclude the images where the patch surrounding the nodule does not lie fully with in the central cropped region of LoDoPAB dataset. For malignancy classification, we consider a BasicResNet model(Al-Shabi et al., 2019) trained on nodule patches from LIDC-IDRI dataset. We utilize the adversarially trained model from (Dröge et al., 2022). We will make the code for our experiments publicly available up on acceptance. In the following f, f_δ, $\hat{u}$ and $\hat{u}_\delta$ denote the clean and adversarial sinogram measurements and the corresponding recovered CT images respectively.

Performance metrics: To measure the adversarial robustness of the reconstruction methods. We measure the PSNR, SSIM and the TV Bregman distance of the reconstructions with clean and adversarial inputs with respect to the ground truth (setting the corresponding subgradient to zero if the norm of the gradient is below a threshold of 10^{-5}, which we consider to be 'numerically zero'). Further, we also measure data consistency of the reconstructions with respect to the clean and adversarial sinograms in terms of PSNR. As it is computationally extremely expensive to derive Lipschitz constant, we empirically compute a lower bound for this as

$$L_b(\mathcal{N}) = \left(\frac{\|\mathcal{N}(f_\delta) - \mathcal{N}(f)\|}{\|\delta\|} \right)_{\max}$$

which is the maximum value obtained across the test set of 100 CT images for the three adversarial noise levels with 5 random restarts (a total of 1500 examples).
For localized attacks, we additionally compare the PSNR values in the local region, and the region exterior to it, for reconstructions with clean and adversarial inputs.

Untargeted Attacks: We perform untargeted attacks (Equation (7)) using step size of $1e-3$ and 20 PGD steps and choose the best adversarial noise from 5 random restarts. The additive perturbations are L_∞ norm bounded by 1%, 2.5% and 5% of the intensity range of the ground truth. The results in Table 1 and Figure 1 demonstrate that in absence of noise, the neural network approaches to CT recovery provide qualitatively better reconstructions

1. https://github.com/oterobaguer/dip-ct-benchmark

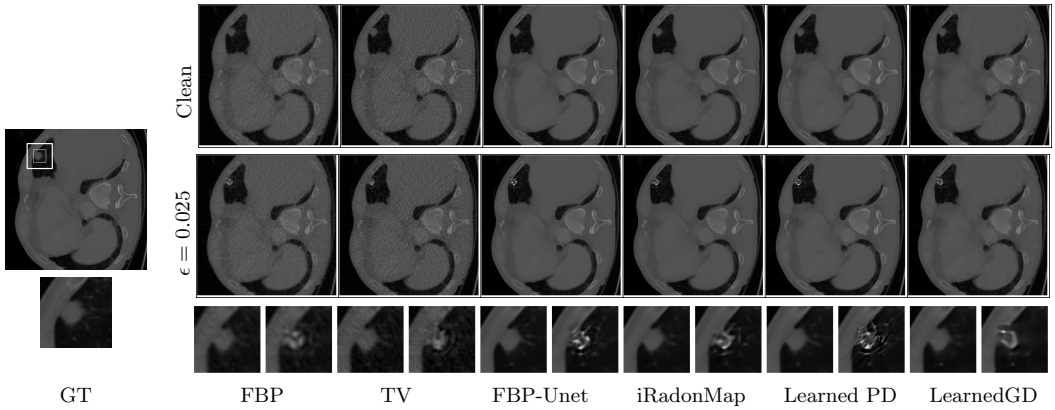

Figure 2: Localized attack on CT reconstruction methods. for $\epsilon = 0.01$.

than FBP and TV minimization. However, their reconstructions are also more susceptible to adversarial perturbations despite using data augmentation with Poisson noise during training. Among the deep learning approaches, the learned primal-dual network which provides the best reconstructions from clean inputs is also the most unstable to perturbations, where as the learned gradient descent is more stable. This is also reflected in the empirical Lipschitz lower bound which is the highest for LearnedPD. This high sensitivity to adversarial attacks is surprising as LearnedPD also encourages data consistency in its (fixed number of) iterations. Among the classical methods, FBP and TV minimization have similar stability in terms of PSNR and L_b, while TV is better in terms of SSIM and Bregman distance as one would have hoped considering the provable stability (6).
Interestingly the adversarial perturbations have a relatively small effect on the data consistency of the recovered CT image for all the methods. The adversarially affected CT reconstructions from LearnedPD with an extremely low average PSNR (0.36 dB) still have a good data consistency (28.7 dB) with the input measurement, showing instabilities typical to unregularized solutions of the recovery problem. Results of similar untargeted attack on LoDoPAB_200 dataset are provided in Table 4 of the appendix.

Transferability of Adversarial Examples: In context of image classification, adversarial perturbations are often transferable across different networks (Liu et al., 2017). Even for CT recovery, we find that generated untargeted perturbations transfer across different methods, detailed results are provided in Table 3 of the appendix.

Localized Attacks: We perform adversarial attacks effecting localized changes Equation (8) using step size of $1e-3$ and iterate for a maximum of 25 PGD steps till the local patch is misclassified. We choose the best adversarial noise from 5 random restarts. To ensure that the degradation remains localized, and to avoid artifacts at the boundary of the local region, we apply a smoothed mask to the adversarial noise setting at every step. The mask is calculated as the sinogram of the Gaussian smoothed spatial mask corresponding to region of interest, and normalized to have maximum value of 1. In Figure 2, reconstructions from different methods with clean and adversarial inputs are compared for a sample image. For each method, the third row shows the cropped patches from the clean (left) and adversarial

(right) reconstructions. The results clearly demonstrate visible alteration in the region of interest $\hat{u}_i$ indicated by the inner square marked in the ground truth image. The predicted malignancy of the region changes for all the methods. Our attack successfully achieves this modification, barely affecting the reconstruction in the exterior region $\hat{u}_e$.

Method	$\hat{u}$ PSNR/SSIM	$\hat{u}_i \vert \hat{u}_e$ PSNR	$(A\hat{u}, f)$ PSNR	ϵ	$\hat{u}_\delta$ PSNR/SSIM	$\hat{u}_{\delta_i} \vert \hat{u}_{\delta_e}$ PSNR	$(A\hat{u}_\delta, f)$ PSNR	$(A\hat{u}_\delta, f_\delta)$ PSNR	(f, f_δ) PSNR	success rate
FBP	30.86/0.787	31.45|30.86	33.81	0.01	30.60/0.782	22.29|30.83	33.79	33.77	55.09	100
				0.025	30.35/0.772	20.93|30.67	33.75	33.42	47.55	100
				0.05	29.97/0.751	19.89|30.34	33.70	32.63	41.08	100
TV	32.36/0.829	31.84|32.37	36.52	0.01	32.00/0.825	22.70|32.32	36.48	36.42	54.77	100
				0.025	31.62/0.812	21.26|32.07	36.46	35.66	46.97	100
				0.05	30.65/0.767	20.28|31.15	36.35	33.59	40.11	100
FBP-Unet	36.94/0.909	35.67|36.95	36.50	0.01	34.85/0.902	19.43|36.61	36.46	36.43	55.11	100
				0.025	33.79/0.889	17.82|35.87	36.37	35.84	47.83	100
				0.05	33.15/0.877	17.27|35.11	36.11	34.42	41.90	100
iRadonMap	35.25/0.888	34.07|35.27	36.09	0.01	33.70/0.883	18.85|35.12	36.03	36.03	55.32	100
				0.025	32.68/0.875	16.53|34.76	35.95	35.52	48.08	100
				0.05	30.60/0.808	15.32|32.73	35.55	33.39	40.81	100
LearnedPD	37.22/0.913	35.97|37.23	36.49	0.01	33.15/0.854	18.34|35.08	36.28	36.10	53.74	100
				0.025	29.90/0.753	16.15|31.57	35.33	34.57	45.41	100
				0.05	25.05/0.559	14.52|25.72	33.29	31.74	38.41	100
LearnedGD	35.80/0.891	34.86|35.82	36.49	0.01	34.86/0.886	22.02|35.71	36.46	36.42	55.29	100
				0.025	34.49/0.883	20.98|35.53	36.42	35.99	48.41	100
				0.05	34.12/0.875	21.11|35.04	36.28	34.72	42.44	100

Table 2: Comparison of robustness to localized attacks on different CT reconstruction method evaluated on 100 samples LoDoPAB testset.

Table 2 summarizes the results of our experiments with localized attacks on different CT reconstruction methods for three levels of adversarial noise. The subscripts i and e denote the restriction to the interior and exterior of the local region to be attacked. Due to masking, the magnitudes of additive perturbation are extremely small, with high PSNR values between the clean and adversarial inputs for all noise levels. Still, our attack is almost always successful in producing local degradations that change the malignancy prediction (success rate of 100 on our test set). This is also reflected in the steep PSNR drop in the local region $\hat{u}_i$, while the PSNR in the exterior region are mostly unaffected. While the classical approaches are more robust to untargeted attacks, they are also sensitive to local changes. This is a direct consequence of ill-posedness of the recovery problem, as we observe nearly similar data consistency of the recovered $\hat{u}_\delta$ with both clean and adversarial inputs. In a recent work (Dröge et al., 2022) demonstrate that the CT images of varying malignancy level can be solutions the same measurement with a high data consistency, but by modifying the reconstruction loss. Our localized attacks also show that the adversarial noise necessary to change the malignancy is very small for a variety of methods and the resulting solutions demonstrate high data consistency with both clean and adversarial inputs.

5. Conclusions

In this work we analyzed the adversarial robustness of CT recovery, for classical and deep learning methods. We showed that deep learning methods are more sensitive to untargeted

adversarial examples than the classical approaches. Even model inspired unrolled networks are susceptible to adversarial examples, even though they encourage data consistency within the network. While the quality of the recovered CT images degrades, we find that the recovered images still exhibit a good degree of data consistency, indicating the need for better regularization of deep learning solutions. In contrast to untargeted perturbations, we find that the classical methods and deep learning methods are similarly affected by adversarial examples targeting small localized regions. Further, we find that such attacks are successful for extremely small perturbations already, such that the resulting reconstructions have high data consistency with original measurements. Therefore, the proposed localized attacks could serve as a way to explore the solution space of reconstruction networks.

References

Jonas Adler and Ozan Öktem. Solving ill-posed inverse problems using iterative deep neural networks. *Inverse Problems*, 33(12):124007, 2017.

Jonas Adler and Ozan Öktem. Learned primal-dual reconstruction. *IEEE Transactions on medical imaging*, 37(6):1322–1332, 2018.

H. K. Aggarwal, M. P. Mani, and M. Jacob. Modl: Model-based deep learning architecture for inverse problems. *IEEE Transactions on medical imaging*, 38(2):394–405, 2018.

Mundher Al-Shabi, Boon Leong Lan, Wai Yee Chan, Kwan-Hoong Ng, and Maxine Tan. Lung nodule classification using deep local–global networks. *International journal of computer assisted radiology and surgery*, 14(10):1815–1819, 2019.

Vegard Antun, Francesco Renna, Clarice Poon, Ben Adcock, and Anders C. Hansen. On instabilities of deep learning in image reconstruction and the potential costs of ai. *Proceedings of the National Academy of Sciences*, 117(48):30088–30095, 2020. doi: 10.1073/pnas.1907377117. URL https://www.pnas.org/doi/abs/10.1073/pnas.1907377117.

Samuel G Armato III, Geoffrey McLennan, Luc Bidaut, Michael F McNitt-Gray, Charles R Meyer, Anthony P Reeves, Binsheng Zhao, Denise R Aberle, Claudia I Henschke, Eric A Hoffman, et al. The lung image database consortium (lidc) and image database resource initiative (idri): a completed reference database of lung nodules on ct scans. *Medical physics*, 38(2):915–931, 2011.

Daniel Otero Baguer, Johannes Leuschner, and Maximilian Schmidt. Computed tomography reconstruction using deep image prior and learned reconstruction methods. *Inverse Problems*, 36(9):094004, 2020.

Hartmut Bauermeister, Martin Burger, and Michael Moeller. Learning spectral regularizations for linear inverse problems. In *NeurIPS 2020 Workshop on Deep Learning and Inverse Problems*, 2020. URL https://openreview.net/forum?id=lUgF584nOSY.

Ashish Bora, Ajil Jalal, Eric Price, and Alexandros G Dimakis. Compressed sensing using generative models. In *International Conference on Machine Learning*, pages 537–546. PMLR, 2017.

M. Burger, E. Resmerita, and L. He. Error estimation for bregman iterations and inverse scale space methods in image restoration. *Computing*, 81(2):109–135, 2007.

H. Chen, Y. Zhang, Mannudeep K Kalra, Feng Lin, Yang Chen, Peixi Liao, Jiliu Zhou, and Ge Wang. Low-dose ct with a residual encoder-decoder convolutional neural network. *IEEE Transactions on medical imaging*, 36(12):2524–2535, 2017.

Zhiqiang Chen, Xin Jin, Liang Li, and Ge Wang. A limited-angle ct reconstruction method based on anisotropic tv minimization. *Physics in Medicine & Biology*, 58(7):2119, 2013.

K. Cheng, F. Calivá, R. Shah, M. Han, S. Majumdar, and V. Pedoia. Addressing the false negative problem of deep learning mri reconstruction models by adversarial attacks and robust training. In *Proc. 3rd Conference on Medical Imaging with Deep Learning*. PMLR, 2020. URL http://proceedings.mlr.press/v121/cheng20a.html.

J. H Choi, H. Zhang, J. H. Kim, C. J Hsieh, and J. S. Lee. Evaluating robustness of deep image super-resolution against adversarial attacks. In *Proc. IEEE/CVF International Conference on Computer Vision*, 2019.

P. L Combettes and J. C Pesquet. Lipschitz certificates for layered network structures driven by averaged activation operators. *SIAM Journal on Mathematics of Data Science*, 2(2): 529–557, 2020.

Mohammad Zalbagi Darestani, Akshay S Chaudhari, and Reinhard Heckel. Measuring robustness in deep learning based compressive sensing. In *International Conference on Machine Learning*, pages 2433–2444. PMLR, 2021.

Hannah Dröge, Yuval Bahat, Felix Heide, and Michael Möller. Explorable data consistent ct reconstruction. In *Proc. British Machine Vision Conference*, 2022.

L. A. Feldkamp, L. C. Davis, and J. W. Kress. Practical cone-beam algorithm. *J. Opt. Soc. Am. A*, 1(6):612–619, Jun 1984. doi: 10.1364/JOSAA.1.000612. URL https://opg.optica.org/josaa/abstract.cfm?URI=josaa-1-6-612.

Kanchana Vaishnavi Gandikota, Paramanand Chandramouli, and Michael Moeller. On adversarial robustness of deep image deblurring. In *2022 IEEE International Conference on Image Processing (ICIP)*, pages 3161–3165. IEEE, 2022.

Yongshuai Ge, Ting Su, Jiongtao Zhu, Xiaolei Deng, Qiyang Zhang, Jianwei Chen, Zhanli Hu, Hairong Zheng, and Dong Liang. Adaptive-net: deep computed tomography reconstruction network with analytical domain transformation knowledge. *Quantitative Imaging in Medicine and Surgery*, 10(2):415, 2020.

M. Genzel, J. Macdonald, and M. März. Solving inverse problems with deep neural networks-robustness included. *IEEE Transactions on Pattern Analysis and Machine Intelligence*, 2022.

I. J Goodfellow, J. Shlens, and C. Szegedy. Explaining and harnessing adversarial examples. In *International Conference on Learning Representations*, 2015.

Harshit Gupta, Kyong Hwan Jin, Ha Q Nguyen, Michael T McCann, and Michael Unser. Cnn-based projected gradient descent for consistent ct image reconstruction. *IEEE Transactions on medical imaging*, 37(6):1440–1453, 2018.

Ji He, Yan Yang, Yongbo Wang, Dong Zeng, Zhaoying Bian, Hao Zhang, Jian Sun, Zongben Xu, and Jianhua Ma. Optimizing a parameterized plug-and-play admm for iterative low-dose ct reconstruction. *IEEE transactions on medical imaging*, 38(2):371–382, 2018.

Ji He, Yongbo Wang, and Jianhua Ma. Radon inversion via deep learning. *IEEE Transactions on medical imaging*, 39(6):2076–2087, 2020.

R Heckel et al. Deep decoder: Concise image representations from untrained non-convolutional networks. In *International Conference on Learning Representations*, 2019.

Yixing Huang, Tobias Würfl, Katharina Breininger, Ling Liu, Günter Lauritsch, and Andreas Maier. Some investigations on robustness of deep learning in limited angle tomography. In *International Conference on Medical Image Computing and Computer-Assisted Intervention*, pages 145–153. Springer, 2018.

Yujia Huang, Huan Zhang, Yuanyuan Shi, J. Zico Kolter, and Anima Anandkumar. Training certifiably robust neural networks with efficient local lipschitz bounds. In *Advances in Neural Information Processing Systems*, volume 34, pages 22745–22757. Curran Associates, Inc., 2021. URL https://proceedings.neurips.cc/paper/2021/file/c055dcc749c2632fd4dd806301f05ba6-Paper.pdf.

Kyong Hwan Jin, Michael T. McCann, Emmanuel Froustey, and Michael Unser. Deep convolutional neural network for inverse problems in imaging. *IEEE Transactions on Image Processing*, 26(9):4509–4522, 2017.

Matt Jordan and Alexandros G Dimakis. Exactly computing the local lipschitz constant of relu networks. In *Advances in Neural Information Processing Systems*, volume 33, pages 7344–7353. Curran Associates, Inc., 2020. URL https://proceedings.neurips.cc/paper/2020/file/5227fa9a19dce7ba113f50a405dcaf09-Paper.pdf.

D. P. Kingma and J. Ba. Adam: A method for stochastic optimization. In *Proceedings of. International Conference on Learning Representations*, 2015.

Shiba Kuanar, Vassilis Athitsos, Dwarikanath Mahapatra, KR Rao, Zahid Akhtar, and Dipankar Dasgupta. Low dose abdominal ct image reconstruction: An unsupervised learning based approach. In *2019 IEEE international conference on image processing (ICIP)*, pages 1351–1355. IEEE, 2019.

Orest Kupyn, Volodymyr Budzan, Mykola Mykhailych, Dmytro Mishkin, and Jiří Matas. Deblurgan: Blind motion deblurring using conditional adversarial networks. In *Proc. IEEE/CVF Conference on Computer Vision and Pattern Recognition*, pages 8183–8192, 2018.

Johannes Leuschner, Maximilian Schmidt, Daniel Otero Baguer, and Peter Maass. Lodopab-ct, a benchmark dataset for low-dose computed tomography reconstruction. *Scientific Data*, 8(1):1–12, 2021.

Yanpei Liu, Xinyun Chen, Chang Liu, and Dawn Song. Delving into transferable adversarial examples and black-box attacks. In *International Conference on Learning Representations*, 2017.

A. Madry, A. Makelov, L. Schmidt, D. Tsipras, and A. Vladu. Towards deep learning models resistant to adversarial attacks. In *International Conference on Learning Representations*, 2018.

T. Meinhardt, M. Moller, C. Hazirbas, and D. Cremers. Learning proximal operators: Using denoising networks for regularizing inverse imaging problems. In *Proc. IEEE/CVF International Conference on Computer Vision*, 2017.

Jan Nikolas Morshuis, Sergios Gatidis, Matthias Hein, and Christian F Baumgartner. Adversarial robustness of mr image reconstruction under realistic perturbations. In *International Workshop on Machine Learning for Medical Image Reconstruction*, pages 24–33. Springer, 2022.

Beverley Newman and Michael J Callahan. Alara (as low as reasonably achievable) ct 2011—executive summary. *Pediatric radiology*, 41(2):453–455, 2011.

Daniël M. Pelt, Kees Joost Batenburg, and James A. Sethian. Improving tomographic reconstruction from limited data using mixed-scale dense convolutional neural networks. *Journal of Imaging*, 4(11), 2018.

J. Radon. On the determination of functions from their integral values along certain manifolds. *IEEE Transactions on Medical Imaging*, 5(4):170–176, 12 1986. ISSN 0278-0062. doi: 10.1109/TMI.1986.4307775.

A. Raj, Y. Bresler, and B. Li. Improving robustness of deep-learning-based image reconstruction. In *International Conference on Machine Learning*, volume 119 of *PMLR*, pages 7932–7942, 2020. URL http://proceedings.mlr.press/v119/raj20a.html.

JH Rick Chang, Chun-Liang Li, Barnabas Poczos, BVK Vijaya Kumar, and Aswin C Sankaranarayanan. One network to solve them all–solving linear inverse problems using deep projection models. In *Proc. IEEE/CVF International Conference on Computer Vision*, pages 5888–5897, 2017.

Emil Y Sidky, Chien-Min Kao, and Xiaochuan Pan. Accurate image reconstruction from few-views and limited-angle data in divergent-beam ct. *Journal of X-ray Science and Technology*, 14(2):119–139, 2006.

Thomas L Slovis. The alara concept in pediatric ct: myth or reality? *Radiology*, 223(1):5–6, 2002.

Yang Song, Liyue Shen, Lei Xing, and Stefano Ermon. Solving inverse problems in medical imaging with score-based generative models. In *International Conference on Learning Representations*, 2022.

Source Method	FBP	FBP-Unet	iRadonMap	LearnedGD	LearnedPD
Clean	30.37/0.738	35.47/0.837	33.94/0.810	34.55/0.815	35.73/0.842
FBP	**18.68/0.194**	16.19/0.139	15.41/0.131	16.04/0.138	16.19/0.151
FBP-Unet	22.03/0.325	**12.19/0.095**	16.33/0.173	17.98/0.279	14.10/0.125
iRadonMap	20.72/0.284	15.18/0.152	**10.86/0.084**	15.45/0.197	16.01/0.171
LearnedGD	21.17/0.375	15.42/0.275	15.96/0.271	**13.90/0.290**	15.28/0.241
LearnedPD	26.39/0.553	25.33/0.604	26.19/0.590	26.23/0.603	**3.38/0.030**
TV	19.19/0.365	16.94/0.289	16.78/0.305	16.66/0.280	16.75/0.333

Table 3: Evaluating transferability of adversarial noises for ϵ=0.025

C. Szegedy, W. Zaremba, I. Sutskever, J. Bruna, D. Erhan, I. Goodfellow, and R. Fergus. Intriguing properties of neural networks. In *International Conference on Learning Representations*, 2014.

Dmitry Ulyanov, Andrea Vedaldi, and Victor Lempitsky. Deep image prior. In *Proc. IEEE/CVF Conference on Computer Vision and Pattern Recognition*, pages 9446–9454, 2018.

Qingsong Yang, Pingkun Yan, Yanbo Zhang, Hengyong Yu, Yongyi Shi, Xuanqin Mou, Mannudeep K. Kalra, Yi Zhang, Ling Sun, and Ge Wang. Low-dose ct image denoising using a generative adversarial network with wasserstein distance and perceptual loss. *IEEE Transactions on Medical Imaging*, 37(6):1348–1357, 2018.

Zhicheng Zhang, Xiaokun Liang, Xu Dong, Yaoqin Xie, and Guohua Cao. A sparse-view ct reconstruction method based on combination of densenet and deconvolution. *IEEE transactions on medical imaging*, 37(6):1407–1417, 2018.

Bo Zhu, Jeremiah Z Liu, Stephen F Cauley, Bruce R Rosen, and Matthew S Rosen. Image reconstruction by domain-transform manifold learning. *Nature*, 555(7697):487–492, 2018.

Appendix A. Transferability of Adversarial Examples

Tranferability of adversarial examples is studied in context of image classification networks, to examine the possibility of black box attacks. We investigate the transferability of adversarial examples across different CT recovery methods, i.e. we test whether, an adversarial example crafted for a "source" CT recovery method also reduces the quality of reconstruction of a different target method for CT recovery. Table 3 summarizes the results of transferability for CT recovery methods, for ϵ value of 0.025. The results demonstrate that the adversarial examples are indeed transferable across different methods to some extent. The adversarial examples for classical methods FBP and TV are highly transferrable across methods significantly reducing the reconstruction quality. The adversarial examples of neural network methods FBP-Unet, iRadonMap and LearnedGD are also transferrable to other network based approaches. The adversarial examples of LearnedPD are least transferable to other methods.

Method	$\hat{u}$ PSNR/SSIM	$(A\hat{u}, f)$ PSNR	ϵ	$\hat{u}_\delta$ PSNR/SSIM	$(A\hat{u}_\delta, f)$ PSNR	$(A\hat{u}_\delta, f_\delta)$ PSNR	(f, f_δ) PSNR	$\|\delta\|^2$	L_b Empir
FBP	28.38/0.649	34.14	0.01	25.26/0.465	33.69	33.69	40.03	0.093	29.69
			0.025	19.77/0.233	31.84	31.75	32.09	0.581	
			0.05	14.36/0.096	28.78	28.52	26.12	2.292	
TV	28.94/0.652	37.47	0.01	24.88/0.520	36.58	36.54	40.10	0.092	33.98
			0.025	18.91/0.302	33.32	33.74	32.20	0.565	
			0.05	13.72/0.126	29.13	30.16	26.33	2.177	
FBP-Unet	33.55/0.799	36.50	0.01	19.37/0.384	34.52	35.244	40.14	0.091	97.56
			0.025	12.82/0.115	28.33	29.23	32.31	0.551	
			0.05	8.38/0.036	23.26	23.97	26.52	2.074	
iRadonMap	32.39/0.778	36.3	0.01	18.46/0.546	30.22	30.58	40.08	0.092	125.21
			0.025	9.40/0.231	19.55	19.88	32.27	0.554	
			0.05	5.39/0.051	14.92	15.12	26.65	2.01	
LearnedPD	33.64/0.802	36.50	0.01	17.75/0.412	34.23	34.92	40.11	0.092	108.48
			0.025	10.56/0.153	31.26	33.08	32.34	0.548	
			0.05	5.94/0.053	31.91	33.66	26.57	2.047	
LearnedGD	32.49/0.776	36.46	0.01	22.44/0.583	35.41	35.67	40.35	0.086	61.95
			0.025	15.66/0.418	32.09	33.01	32.72	0.499	
			0.05	10.89/0.301	29.10	30.02	27.19	1.773	

Table 4: Comparison of robustness to untargeted attacks on different CT reconstruction methods using 20 attack iterations on 100 samples LoDoPAB200 testset.

Appendix B. Additional Results

Untargeted Attacks on LoDoPAB_200 Table 4 summarizes the results of our untargeted attacks on LoDoPAB_200 dataset, where the measurements are generating using 200 projection beams. Similar to our results on the LoDoPAB dataset, we find that classical approaches are more robust to untargeted attacks. However, on this dataset, the fully learned approach of iRadon Map is the most unstable method, followed by LearnedPD. LearnedGD is stable among the network based methods. Further, the methods show a trend of have a higher value of L_b on LoDoPAB_200 dataset in comparison with LoDoPAB dataset indicating higher instabilities as the reconstruction from 200 projection beams is more severely ill-posed than from 513 projections.

Qualitative Results Figure 3 shows the results of untargeted attack on two example CT images for three adversarial noise levels. The clean and adversarial reconstructions for the methods are shown. The visual results also indicate relative robustness of classical approaches to untargeted attacks.

Figure B shows result of localized attack on an example CT image for adversarial noise level of 0.01. The adversarial noise that produces the localized changes is also depicted. We can observe that the attack successfully modifies the local region using extremely low noise level. Figure 5 shows the results of localized attacks on 20 example CT images in

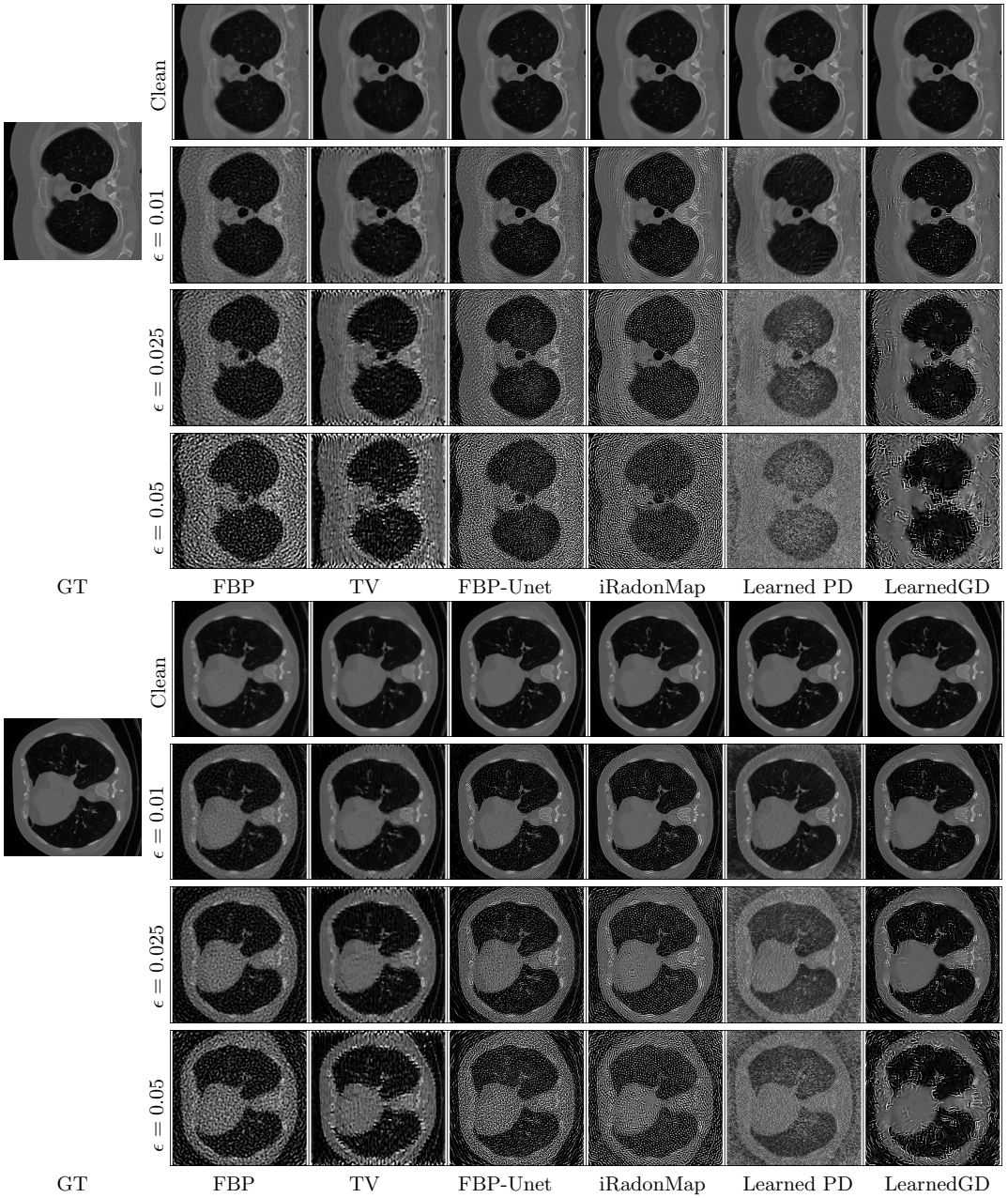

Figure 3: Untargeted attack on CT reconstruction methods for ϵ values 0.01, 0.025 and 0.05.

LoDoPAB test set. For each method, the local patches extracted from clean and adversarial reconstructions are shown.

Figure 4: Localized attack on CT reconstruction methods. for $\epsilon = 0.01$. Error map multiplied by $\times 25$ for visibility.

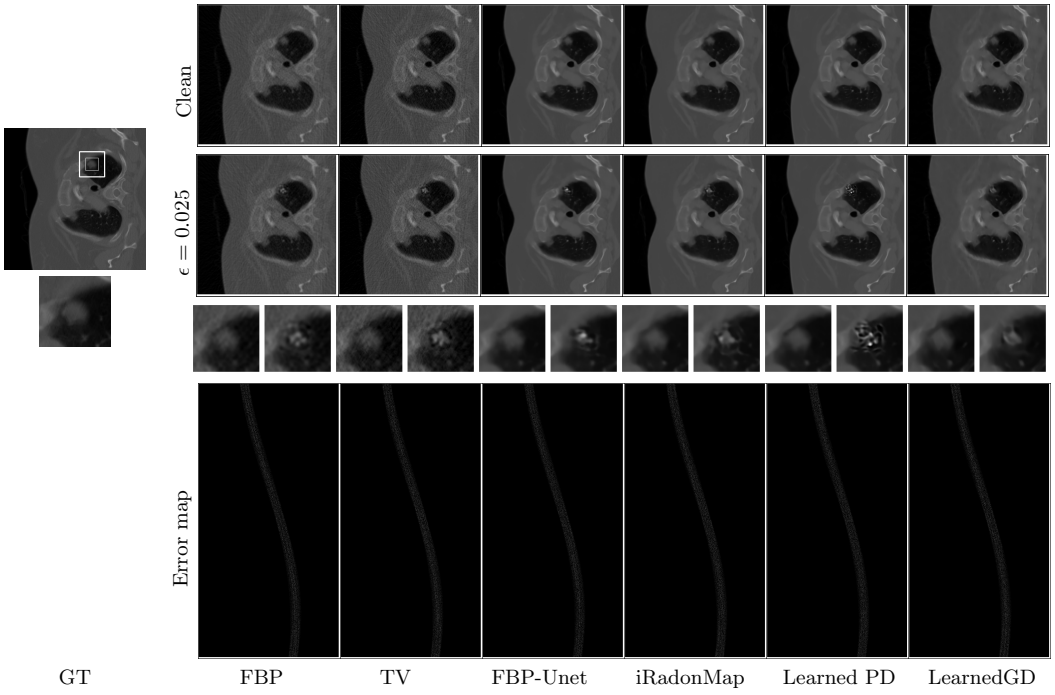

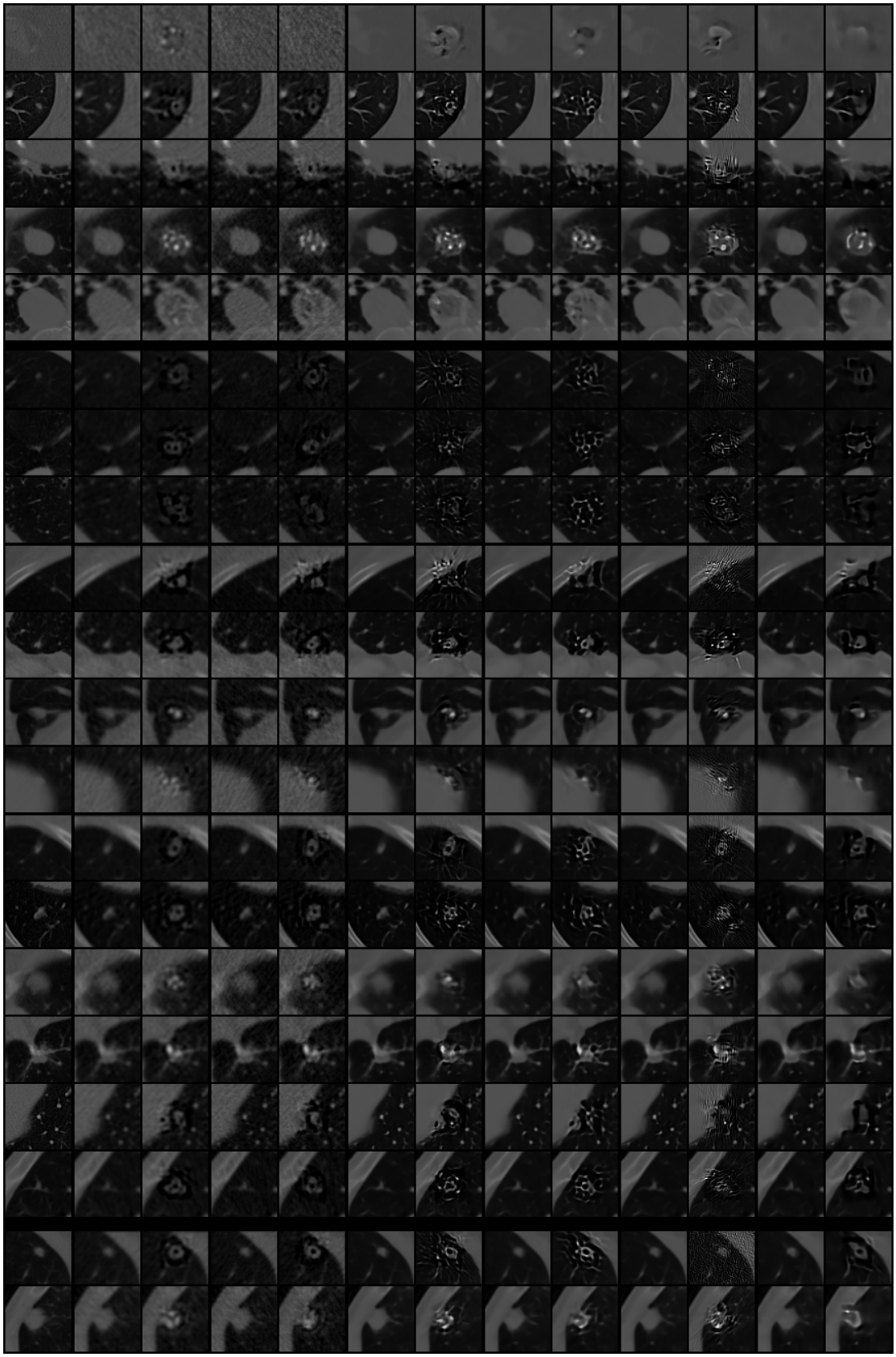

Figure 5: Result of localized attacks on 20 images. For each method left patch is from clean reconstruction and right is the result of attack.